Applied Geochemistry 135 (2021) 105117

Contents lists available at ScienceDirect

Applied Geochemistry

journal homepage: www.elsevier.com/locate/apgeochem

Adsorption of barium and radium on montmorillonite: A comparative experimental and modelling study

Martina Klinkenberg [a,*], Felix Brandt [a], Bart Baeyens [b], Dirk Bosbach [a], Maria Marques Fernandes [b,**]

[a] Institute of Energy and Climate Research (IEK-6) – Nuclear Waste Management and Reactor Safety, Forschungszentrum Jülich GmbH, 52425, Jülich, Germany
[b] Paul Scherrer Institut, Laboratory for Waste Management, 5232, Villigen PSI, Switzerland

ARTICLE INFO

Editorial handling by Dr. Z Zimeng Wang

Keywords:
Radium
Barium
Adsorption
Modelling
Cation exchange
Selectivity
Montmorillonite

ABSTRACT

The widely favored option for the safe storage of high-level radioactive waste is a multi-barrier disposal system with clay-based geotechnical barriers e.g. bentonite. Montmorillonite as a major constituent of bentonite (up to 90 wt.-%) is an important sink for potentially released radionuclides. The adsorption of ^{226}Ra and Ba on Na-montmorillonite (SWy-2) was investigated as function of pH (edges) and of Ba concentration (isotherms) at different ionic strengths. Ba is often used as a chemical analogue for ^{226}Ra due to their closely related physical and chemical properties e.g. the formation of complete Ba/Ra solid solutions. The experimental Ba/Ra adsorption data could be quantitatively described by considering cation exchange reactions on the planar sites of montmorillonite. To describe the pH dependent adsorption of Ba and Ra at high ionic strength and high pH, an additional reaction involving surface complexation was necessary. The fitted selectivity coefficients (K_c) for the cation exchange of Ba and Ra with respect to Na are very similar at low ionic strength (0.02 M), whereas at higher ionic strength (0.3 M), Ra appears to be more selective.

1. Introduction

Scientific experts and waste management organizations consider the direct disposal of spent nuclear fuel in deep geological formations as the best option for closing the nuclear energy cycle (SKB, 2011; Nagra, 2014; Ewing, 2015). To ensure the long-term safety of an underground repository, the fate of important radionuclides must be assessed in geochemical scenarios. Some of these scenarios examine the consequences of contact with the interstitial "*in situ*" porewaters with spent nuclear fuel and indicate that ^{226}Ra can become a main contributor to the total dose after 10^4–10^5 years of waste disposal (SKB, 2011). In addition, in the context of environmental and mining questions, ^{226}Ra is regarded as an important contributor to naturally occurring radioactive materials (NORM) and to the environmental hazards associated with these (Rutherford et al., 1996; Fisher, 1998; Martin et al., 2003; Zhang et al., 2015; Gusa et al., 2020; Silva et al., 2020).

Some recent studies have focused on the formation of secondary ^{226}Ra containing mineral phases via co-precipitation or recrystallization as a retention mechanism (Rosenberg et al., 2014; Curti et al., 2010; Klinkenberg et al., 2018; Heberling et al., 2018). However, adsorption also needs to be accounted for in safety assessments. In this respect, 2:1 clay minerals are important due to their structure, permeability, swelling, and cation exchange capacities. In the open literature, studies on the adsorption of ^{226}Ra on clay minerals are sparse. Boscov et al. (2001) observed significant retention of ^{226}Ra in diffusion experiments with a lateritic clay soil. Hidaka et al. (2007) provided geochemical evidence that ^{226}Ra preferentially adsorbs to clay minerals in the surroundings of the Oklo uranium deposit, considered as a natural fission reactor.

Bentonites are envisaged as engineered barriers in underground waste disposal concepts (e.g. Nagra, SKB). In the Swiss concept (Nagra, 2002), bentonite is foreseen as a buffer material to seal waste canisters, while bentonite-sand mixtures are foreseen as backfill material for access tunnels (Jenni et al., 2019). Montmorillonite is the main constituent of bentonite and a common mineral in soils and sediments. Komarneni et al. (2001) investigated the removal of ^{226}Ra by synthetic Na-micas and natural montmorillonites. Both types of clay minerals showed ^{226}Ra uptake. In addition, in some of their experiments, Komarneni et al.

* Corresponding author.
** Corresponding author.
E-mail addresses: m.klinkenberg@fz-juelich.de (M. Klinkenberg), maria.marques@psi.ch (M.M. Fernandes).

https://doi.org/10.1016/j.apgeochem.2021.105117
Received 9 July 2021; Received in revised form 7 September 2021; Accepted 11 September 2021
Available online 23 October 2021

(2001) considered Ba adsorption and used Ba as an analogue for ^{226}Ra. Chen and Kocar (2018) investigated the adsorption of ^{226}Ra on montmorillonite, pyrite and iron hydroxides for a range of pH values and common background electrolytes. Ra adsorption was observed onto all minerals, but varied according to the mineral, solution pH and specific competing cations.

For the prediction of the adsorption of metal cations onto montmorillonite, a two site non-electrostatic surface complexation and cation exchange (2SPNE SC/CE) model was developed based on large sets of experimental data on purified montmorillonite and successfully applied (Fernandes and Baeyens, 2019; Bradbury & Baeyens, 1997, 2005). So far, only Chen and Kocar (2018) attempted to derive a model for the adsorption of ^{226}Ra on montmorillonite, applying the Bradbury and Baeyens (1997) approach in the case of sodium montmorillonite. However, the isotherm and background electrolyte fitted log K_c reproduced the experimental data not to the satisfaction of that study's authors, especially when compared to the modelling of iron (hydr)oxides in the same study.

In this study, new experimental and modelling data to improve the quantitative understanding of the adsorption of ^{226}Ra and Ba on montmorillonite are reported. Due to the chemical similarity, Ba is often considered as a chemical analogue for ^{226}Ra. To test the use of Ba as a chemical analogue for ^{226}Ra with respect to sorption on montmorillonite similar experiments (i.e., with the same clay mineral and the experimental setup) were carried out with Ba and ^{226}Ra.

2. Materials and methods

2.1. Preparation and conditioning of montmorillonite suspensions

The Na-montmorillonite suspensions were prepared following the procedure as described in Baeyens and Bradbury (1995). A Na-montmorillonite SWy-2 (Newcastle formation, County of Crook, Wyoming, USA) purchased from the Clay Minerals Society source clay repository (Society), was washed several times with 1 M NaCl to purify it from soluble salts and calcite and to convert it into a homoionic Na-montmorillonite. A grain size fractionation by centrifugation and peptization to obtain the fraction <0.5 μm was carried out and soluble hydroxy aluminum compounds and other acid soluble impurities were removed by washing the clay suspension with a 0.1 M NaCl solution at pH 3.5 for 1 h. The exact clay content of the Na-SWy was determined by drying to a constant weight at 105 °C and correcting for the salt content. The cation exchange capacity (CEC) of the SWy was determined in earlier studies by the Na isotopic dilution method at neutral pH and yielded a value of 870 ± 35 meq·kg^{-1} (Baeyens and Bradbury, 1997). A detailed characterization of the SWy source clay is given in Van Olphen and Fripiat (1979).

2.2. Batch adsorption experiments

Three types of adsorption experiments were performed: (i) pH dependent adsorption of trace ^{226}Ra and of trace Ba as a function of pH at different ionic strengths (IS); (ii) concentration dependent adsorption of Ba (isotherms) at constant pH and ionic strength; (iii) measurements of the adsorption of trace ^{226}Ra as a function of increasing Ba concentrations (along the Ba isotherm). No adsorption isotherm was determined only with ^{226}Ra. However, if both trace ^{133}Ba and trace ^{226}Ra show similar adsorption with increasing Ba concentration, they can be considered as chemical analogues with respect to adsorption on montmorillonite. All adsorption edges and isotherms were carried out at room temperature (21 ± 2 °C) and under atmospheric air conditions.

Analytical grade chemicals and ultrapure deionized water (18.2 MΩ cm^{-1} at 25 °C) were used to prepare all solutions. The radioactive tracer solutions of ^{133}Ba and ^{226}Ra were prepared from well-characterized stock solutions. The ^{133}Ba ($t_{1/2}$ = 10.55 a) stock solution was purchased from Eckert and Ziegler, Isotope Products Laboratories (California, USA) and diluted in deionized water to produce an acidic stock solution (pH ~1). The ^{226}Ra ($t_{1/2}$ = 1600 a) stock solution (5 · 10^{-5} mol L^{-1}) was prepared from $RaBr_2$ and measured against an independent standard.

^{133}Ba stock solutions for use in the adsorption experiments were prepared by labelling aliquots of the radiotracer stock solution in the given background electrolyte. The tracers were diluted from the stock solution and added to the clay suspension at the beginning of the experiments. Samples were prepared in 50 mL polyethylene centrifuge tubes in duplicates. Specific details for each type of experiment are provided in sections 2.2.1 and 2.2.2. The centrifuge tubes were mounted into end-over-end shakers to react for 7 days. The duration of 7 days was chosen based on kinetic experiments at pH = 7 (Fig. S1 and Table S1) Phase separation was obtained using a Beckman Coulter Avanti™ J30i High-Performance centrifuge (1 h at 108,000 g max. at 25 °C) or Heraeus Multifuge SR3+ (Thermo Scientific; 1 h at 3000 g at 20 °C) and aliquots of the supernatants were analyzed for their elemental concentrations. The pH of each sample was measured using a Metrohm combined electrode calibrated against commercially available buffers.

2.2.1. pH dependent adsorption

Adsorption edges were obtained by equilibrating trace concentrations of (^{133}Ba + ^{137}Ba) or ^{226}Ra with Na-SWy from the acidic to the basic pH range at ionic strengths of 0.02 M–0.3 M (Table 1). Stable ^{137}Ba was used as a carrier for ^{133}Ba to adjust the total Ba concentrations. Different buffers (Sigma-Aldrich) at concentrations of 2·10^{-3} M were used to prevent a pH drift in the adsorption experiments: $C_6H_{13}NO_4S$ (MES, for pH = 5.5, 6.2 and 6.8), $C_7H_{15}NO_4S$ (MOPS, for pH = 7.3), $H_2NC(CH_2OH)_3$ (TRIS, for pH = 7.9 and 8.5), or $C_8H_{17}NOS$ (CHES, for pH = 9.2 and 9.8). The pH was adjusted with 1 M NaOH and 1 M HNO_3, respectively. The ionic strength was generally not affected by the adjustment of the pH. For comparison with the experiments where the pH was kept constant by addition of a buffer, experiments were carried out with ^{226}Ra which were pH-adjusted with NaOH, only.

2.2.2. Adsorption isotherms

Ba adsorption isotherms were collected by labelling stable Ba solutions in the required concentrations with ^{133}Ba with a fixed pH = 7.0 (MOPS buffer) and ionic strength of 0.02 M NaCl (Table 1, details provided in Table S7). Each standard solution containing ^{133}Ba was equilibrated at least overnight before use to avoid tracer wall adsorption interference.

The adsorption of trace ^{226}Ra as a function of increasing Ba concentration was measured by labelling stable Ba solutions in the required concentrations with ^{226}Ra, with a fixed pH = 7.0 (MOPS buffer) and ionic strength of 0.02 M NaCl.

2.3. Analytical methods

The activity of ^{133}Ba was determined from radio-assays of aliquots of the supernatants as well as of the labelled standard solutions prepared simultaneously at the start of the adsorption experiments using a Canberra Packard Cobra Quantum gamma counter. The concentration of ^{226}Ra was determined by LSC-measurements using the ultra low level liquid scintillation spectrometer Quantulus (Perkin Elmer, USA). For the analyses, 1 mL aliquots of the supernatants as well as of the labelled standard solutions were mixed with 19 mL of Ultima Gold LLT cocktail (Perkin Elmer, USA). The LSC-glass vials were glued gas tight with epoxy resin to avoid the release of Rn. The measurement of the samples was carried out after 38 days in equilibrium condition of ^{226}Ra and Rn.

The initial and equilibrium concentrations of ^{137}Ba in the combined Ba/^{226}Ra experiment were analyzed using an ICP-MS ELAN 6100 DRC (PerkinElmer SCIEX) instrument after dilution and acidification with HNO_3.

Table 1
Summary of Ba and ^{226}Ra adsorption experiments on Na-SWy.

		Type of experiment	$[X^{a}]_{init/eql}$ (M)[b]	Ionic strength NaCl (M)	S/L (g L^{-1})	pH
1	^{133}Ba	Edge	$3.3{\cdot}10^{-8}$ - $3.9{\cdot}10^{-8}$	0.03	2.91	3.3–9.3
2	^{133}Ba	Edge	$4.3{\cdot}10^{-8}$ - $3.7{\cdot}10^{-8}$	0.3	2.96	2.6–10.6
3	^{226}Ra	Edge	$2.0{\cdot}10^{-7}$	0.02	2.21	5.5–10.2
4	^{226}Ra	Edge	$1.9{\cdot}10^{-8}$	0.14	8.33	5.6–10.2
5	^{226}Ra	Edge	$1.8{\cdot}10^{-8}$	0.3	13.95	5.7–9.9
6	^{137}Ba/^{133}Ba	Isotherm	$2.03{\cdot}10^{-9}$ - $1.8{\cdot}10^{-2}$	0.02	0.88–4.39	6.9–7.1
7	^{137}Ba/^{226}Ra	Isotherm	[^{137}Ba] 0.0–$1.7{\cdot}10^{-2}$	0.02	0.84–4.29	6.5–7.0
		Isotherm	[^{226}Ra] $4.3{\cdot}10^{-9}$ - $5.9{\cdot}10^{-9}$			

[a] X = Ba or Ra; [b]For edges initial concentrations and for isotherms equilibrium concentrations are given.

2.4. Adsorption modelling

The adsorption of Ra and Ba on Na-montmorillonite is mainly controlled by Ra^{2+}-Na^{+} and Ba^{2+}-Na^{+} cation exchange reactions on the planar sites. These cation exchange reactions can be written as follows:

$$2\text{Na-mont.} + Me^{2+} \Leftrightarrow \text{Me-mont.} + 2\ Na^{+} \quad (1)$$

with Me^{2+} being Ra^{2+} or Ba^{2+}. To describe the reaction in terms of a so-called selectivity coefficient a mass action law is normally used. Depending on the way in which the adsorbed and aqueous quantities are treated, different values for selectivity coefficients for the same data sets can be obtained. According to the Gaines and Thomas convention (Gaines and Thomas, 1955) which uses the fractional scale for the adsorbed cations and the molarity scale for the cations in solution, the selectivity coefficients (K_c) can be defined as:

$$^{X}_{Na}Kc = \frac{N_{Me}}{N_{Na}^{2}} \cdot \frac{[Na]^{2}}{[Me]} \cdot \frac{(\gamma_{Na})^{2}}{(\gamma_{Me})} \quad (2)$$

where N_{Me} and N_{Na} are the equivalent fractional occupancies, defined as the equivalent of Na or Me (i.e. Ra or Ba) adsorbed per kg of clay mineral divided by the cation exchange capacity (CEC) [eq·kg^{-1}]; [Na] and [Me] are the aqueous molar concentrations (M) and γ_{Na} and γ_{Me} are aqueous phase activity coefficients. By fitting the experimental data with the aforementioned cation exchange reactions, the selectivity coefficients for the cation exchange of Ba^{2+} and Ra^{2+} with respect to Na^{+} on the planar sites of montmorillonite were derived.

To model the experimental data at higher ionic strength and pH > 8, an additional adsorption mechanism had to be considered. In this case the 2 site protolysis non-electrostatic surface complexation (2SPNE SC/

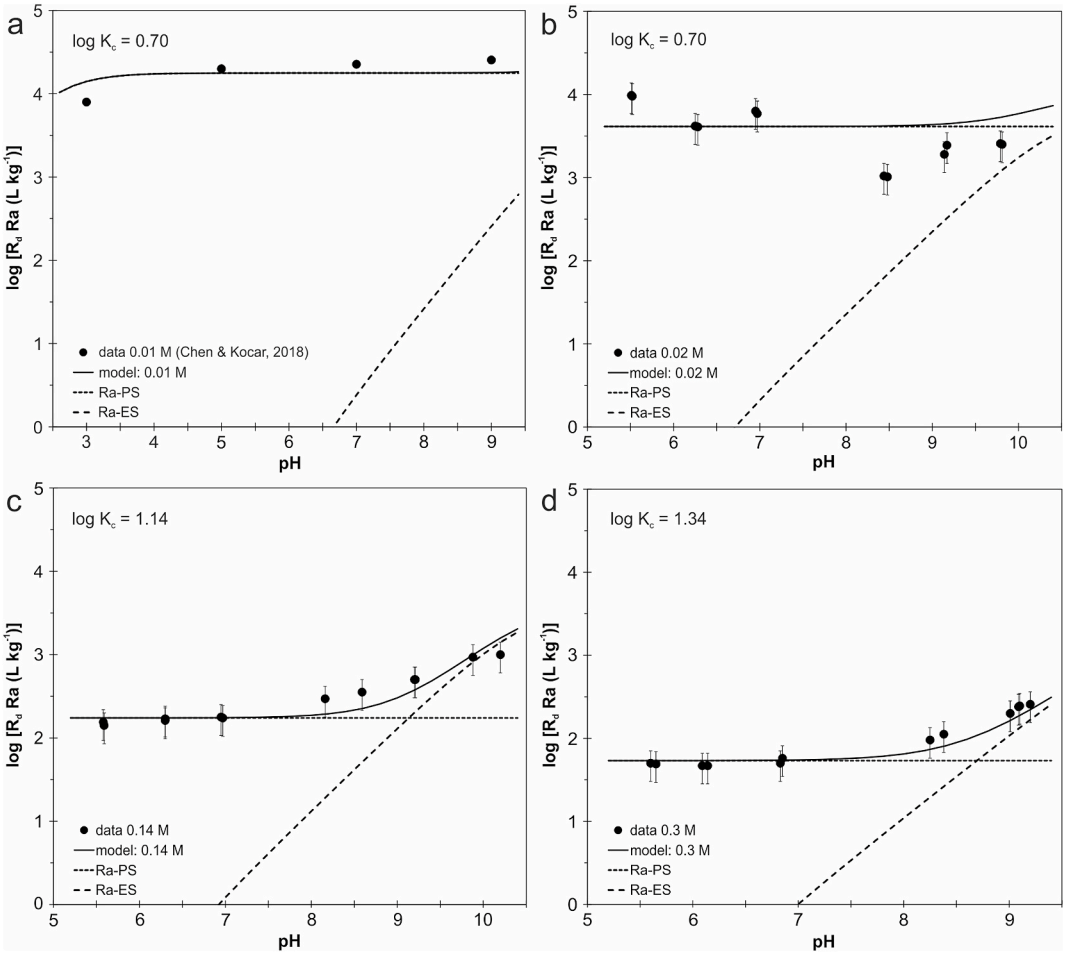

Fig. 1. Experimental and modelled results of pH-edges of a) ^{226}Ra on Na-montmorillonite in 0.01 M NaCl (experimental data taken from Chen and Kocar, 2018), b) ^{226}Ra on Na-SWy-2 in 0.02 M NaCl, c) ^{226}Ra on Na-SWy-2 in 0.14 M NaCl, d) ^{226}Ra on Na-SWy-2 in 0.3 M NaCl. Ra-PS = planar sites; Ra-ES = edge sites.

CE) model (Bradbury and Baeyens, 1997) was applied. The uptake of Ra/Ba was described by surface complexation on the amphoteric edge sites of the montmorillonite platelets. The type of sites, the capacity and protolysis constants of these sites are defined in the 2SPNE SC/CE model. The surface complexation constants for ^{226}Ra and Ba have been derived in this study from the experimental data. These thermodynamic calculations were performed with the code MINSORB (Bradbury and Baeyens, 1997), which is derived from geochemical code MINEQL (Westall et al., 1976) and which contains subroutines for calculating CE and SC reactions simultaneously. Aqueous activity coefficients are calculated using the Davies relation (Davies, 1962) with a value of 0.3 for the C_D constant.

3. Results and discussion

To avoid unnecessary repetition, the experimental results of the ^{226}Ra and Ba pH edges and isotherms are presented and discussed separately from the modelling results but combined in Fig. 1 to Fig. 3. Symbols represent the experimental data, continuous lines represent the calculated overall adsorption and the broken lines are the contributions of the individual surface species to the total adsorption. All experimental and model data are provided in tables A1 to A9 of the appendix and in Tables S1–S9 of the supplementary materials.

3.1. Experimental results of the pH dependent adsorption on Na-SWy

The adsorption of metals (Me) is usually quantified by the solid-liquid distribution ratio R_d, which is defined as:

$$R_d = \frac{[Me_{init}] - [Me_{eql}]}{[Me_{eql}]} \cdot \frac{V}{m} \quad (3)$$

with $[Me_{init}]$, the total (active + inactive) initial aqueous metal concentration (M); $[Me_{eql}]$, the total (active + inactive) equilibrium aqueous metal concentration (M); V the volume of the liquid phase (L), and m the mass of solid phase (kg). Based on error propagation, the experimental error of R_d was estimated to be ±40%.

Kinetic experiments were carried out and showed that the experimental time of 7 days is sufficient (Fig. S1 and Table S1 of the supplements). The ^{226}Ra data above pH = 9 are from experiments without a buffer, resulting in similar R_d as the buffered experiments at the same final pH. The ^{226}Ra adsorption edges on Na-SWy determined in 0.02 M, 0.14 M and 0.3 M NaCl, together with the data from Chen and Kocar (2018) in 0.01 M NaCl, are shown in the Fig. 1. Generally, for all systems the adsorption shows no pH dependency up to pH 8 and increases as a function of decreasing ionic strength. The increase of adsorption with decreasing ionic strength is typical for cation exchange reactions due to competitive effects of the background cation, see equation (2) (e.g. Tertre et al., 2011a,b).

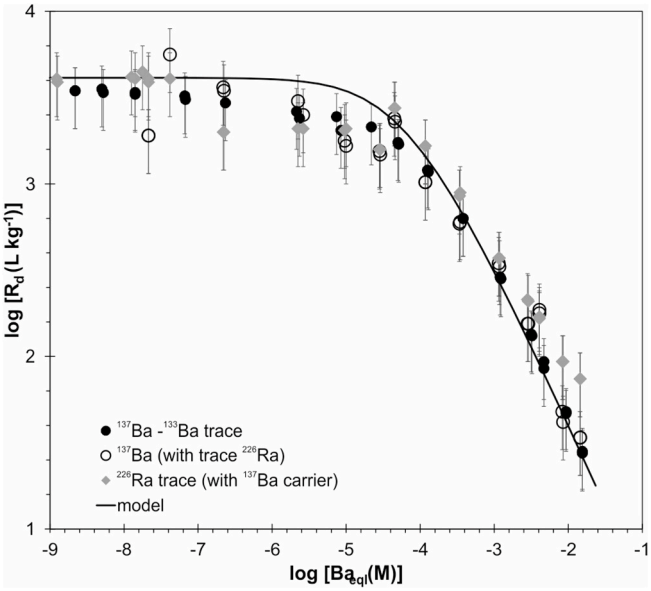

Fig. 3. Adsorption isotherms of ^{137}Ba/^{133}Ba trace and ^{137}Ba/^{226}Ra trace on Na-SWy at I = 0.02 M NaCl and pH 7.

At higher ionic strengths and pH > 8 (Fig. 1 c,d), the adsorption increases as a function of pH. A similar pH dependency was observed by Tachi et al. (2001) on purified smectite in 0.1 M NaCl. Ames et al. (1983) reported experimental values for the sorption of ^{226}Ra on montmorillonite at 25 °C in 0.01 M NaCl. Considering the difference in ionic strength, their results are in good agreement with the results presented here at 0.02 M.

The Ba adsorption edges on Na-SWy in 0.03 M and 0.3 M NaCl show a very similar trend as the ^{226}Ra data (Fig. 2). At low ionic strength, also, the log R_d values of ^{226}Ra and Ba are very close, whereas at 0.3 M the Ba edge is systematically lower than the ^{226}Ra edge (data are similar within uncertainties).

3.2. Experimental sorption results of isotherms on Na-SWy

One Ba adsorption isotherm on Na-SWy in 0.02 M NaCl and pH = 7 was determined using ^{133}Ba as isotopic tracer to monitor stable ^{137}Ba concentrations in the liquid phase after equilibrium. The results are

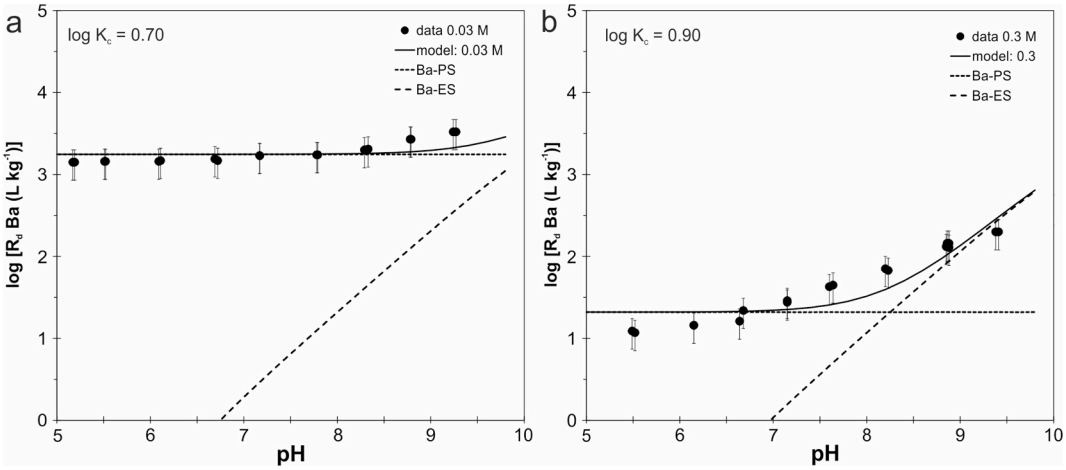

Fig. 2. Experimental and modelled results of pH-edges of a) Ba on Na-SWy-2 at 0.03 M NaCl and b) Ba on Na-SWy-2 in 0.3 M NaCl.

shown as log R_d values versus [Ba_{eql}] concentrations in Fig. 3. This Ba isotherm was repeated in a separate experiment (open circles in Fig. 3) under the same experimental conditions, using ^{137}Ba as a carrier for a ^{226}Ra tracer. Here, the Ba concentration in the liquid phase after sorption was analytically determined using ICP-MS. The isotherm of ^{137}Ba in this experiment is identical within the experimental error with the independently determined $^{133}Ba/^{137}Ba$ isotherm (full circles in Fig. 3).

The shape of the Ba isotherms is characteristic of a Langmuir type behaviour where the adsorption is linear in the low concentration range for [Ba_{eql}] $< 10^{-5}$ M and becomes non-linear at higher [Ba_{eql}] because of site saturation. The amount of Ba adsorbed at the highest [Ba_{eql}] concentration corresponds to 0.4 mol kg^{-1}, or 0.8 eq kg^{-1} Ba^{2+}, which represents ~90% of the Na-CEC of SWy montmorillonite.

The adsorption of trace ^{226}Ra as measured along the ^{137}Ba isotherm (i.e. as a function of Ba concentration) under similar conditions is shown in Fig. 3 (grey diamonds) as log R_d vs [Ba_{eql}] concentrations. As for the cases where only Ba was used in the experiments, the isotherms follow an overall non-linear trend, with a plateau of log R_d at low total Ba concentrations for [Ba_{eql}] $< 10^{-5}$ M and a linear decrease for [Ba_{eql}] $> 10^{-4}$ M. A comparison of the data points with the Ba isotherms shows that ^{137}Ba behaves as an ideal carrier for the ^{226}Ra tracer as all three sets of data match within experimental error (Fig. 3).

Chen and Kocar (2018) carried out ^{226}Ra isotherms at I = 0.01 M NaCl in the ^{226}Ra concentration range between [^{226}Ra] = ~10^{-11} M and 10^{-12} M, thus covering one order of magnitude of the isotherm. For this range they determined a linear relationship between ^{226}Ra adsorbed and ^{226}Ra in solution. The log R_d values presented here (Fig. 3) are coherent with their observed Ra concentrations if ionic strength and S/L are taken into account (Chen and Kocar, 2018).

3.3. 3.3. Modelling results of pH-edges and isotherms for Ba and Ra adsorption on Na-SWy

As already mentioned in section 3.2, the majority of the ^{226}Ra and Ba adsorption data can be quantitatively described by a straightforward cation exchange mechanism. The only non-adjustable parameter in the cation exchange model is the cation exchange site capacity (Na-CEC = 0.87 eq kg^{-1}). The dotted curves in Figs. 1 and 2 represent the contribution of cation exchange to the total adsorption for Ra and Ba obtained with the best-fit selectivity coefficients tabulated in Table 2 for the corresponding experimental data sets. As can be seen from the model curves (dotted lines), most of the ^{226}Ra (Fig. 1) and Ba (Fig. 2) data is covered by cation exchange. In the case of Ba, the log K_c values are slightly higher for the edge data set at 0.02 M in comparison to 0.3 M NaCl. On the other hand, for ^{226}Ra there is clear trend that the log K_c values are increasing as a function of the NaCl background concentrations. The reason why this dependency is more pronounced for ^{226}Ra than for Ba is not known but could be caused by the difference in ionic radius of both divalent earth-alkaline cations. The effective ionic radii for the 12 fold coordination is 1.61 Å and 1.70 Å for Ba^{2+} and Ra^{2+}, respectively (Shannon, 1976). One would expect that the Molar Gibbs Energy of ion hydration ($\triangle G_{hydration}$) would be smaller for Ra compared to Ba which would explain the higher selectivity of Ra compared to Ba (Teppen and Miller, 2006). However, the only source the authors could find for the $\triangle G_{hydration}$ for Ra is given by Marcus (1991) who tabulates the same value for Ra^{2+} and Ba^{2+}, i.e. $\triangle G_{hydration} = -1250$ kJ mol^{-1}. Nonetheless, based on the higher ionic radius of Ra one could postulate a selectivity behavior which is more pronounced in higher ionic strength media. Van Loon and Glaus (2008) measured a higher selectivity coefficient for Cs with respect to Na at higher ionic strength than at lower ionic which they explained by the reduction of the interlayer space and the accumulation of weakly hydrated Cs in the interlayer space and Na in the bulk water.

At low ionic strength (NaCl ≤0.02 M) the Ra and Ba K_c values are very consistent and both metals can be considered to behave as chemical analogues regarding cation exchange. This is further confirmed by the Ba adsorption isotherm with ^{226}Ra as radiochemical tracer. The ^{137}Ba isotherm obtained either by using ^{133}Ba or ^{226}Ra radiotracers are nearly congruent. The model curve also indicates that the Ba and ^{226}Ra data is perfectly described with a log K_c value of 0.7 which is also consistent with the pH edge data (see Table 2).

From the experimental data presented in Figs. 1 to 3 there is a more pronounced adsorption for both Ra and Ba under certain conditions. At high pH and high ionic strength, the cation exchange mechanism cannot describe the increase of the experimental R_d values. For these data points, a second adsorption mechanism is postulated in which the adsorption of Ba and Ra is governed by surface complexation. The 2SPNE SC/CE sorption model developed for montmorillonite (Bradbury and Baeyens, 1997) was used to describe the additional Ra/Ba uptake at high pH and ionic strength.

The montmorillonite specific non-adjustable parameters (i.e., site capacity, protolysis reactions and constants) (Bradbury and Baeyens, 1997) together with the fitted SC reactions and constants for Ba/Ra are given in Table 3.

Because Ba and Ra have a very weak hydrolysis behavior, the adsorption was assumed to take place on the second category of weak sites ($\equiv S^{W2}OH$) which have protolysis constants describing the amphoteric behavior in the alkaline region of the titration curves (see Bradbury and Baeyens, 1997). The only parameter that needed to be fitted is the surface complexation reaction of Ba and ^{226}Ra on this type of site. The best fit log ^{SC}K value of −5.0 could quantitatively describe the Ba and Ra data well. This is shown by the solid lines in Figs. 1 to 3 which represent the total modelled Ba and ^{226}Ra adsorption on montmorillonite. The contribution of the adsorption by surface complexation is illustrated by the dashed lines. Note that in case pH is below 8 and ionic strength below 0.1 M, the adsorption by cation exchange is dominant and the contribution by surface complexation becomes negligible.

4. Conclusions

The adsorption of ^{226}Ra and Ba onto Na-montmorillonite, which is key component of the technical barrier system in future high-level radioactive waste repositories, was investigated with respect to the effect of pH and ionic strength.

The experimentally obtained adsorption isotherms at fixed pH and

Table 2
Summary of selectivity coefficient for Ba/Ra–Na exchange on montmorillonite.

Experiment	Kinetics		**Edges**				**Isotherms**
NaCl concentration (M)	0.02	0.1	0.01	0.02	0.14	0.3	0.02
Cation exchange reaction	log K_c						
2Na-SWy + Ba^{2+} ⇔ Ba-SWy + $2Na^+$	–	–	–	0.70	–	**0.90**	**0.70**
2Na-SWy + Ra^{2+} ⇔ Ra-SWy + $2Na^+$	0.84	1.34	0.70	0.70	1.14	1.34	0.70

Table 3
Capacity value and protolysis reactions/constants for the $S^{W2}OH$ sites on Na-montmorillonite (Bradbury and Baeyens, 1997) in the 2SPNE SC/CE adsorption model and the derived SC reactions and constants for Ba and Ra.

Site type	Capacity
$\equiv S^{W2}OH$	$4.0 \cdot 10^{-2}$ mol·kg^{-1}
Surface complexation reactions	**Constants**
$\equiv S^{W2}OH + H^+ \Leftrightarrow \equiv S^{W2}OH_2^+$	log $K^+ = 6.0$
$\equiv S^{W2}OH \Leftrightarrow \equiv S^{W2}O^- + H^+$	log $K^- = -10.5$
$\equiv S^{W2}OH + Ba^{2+} \Leftrightarrow \equiv S^{W2}OBa^+ + H^+$	log $K_1 = -5.0$
$\equiv S^{W2}OH + Ra^{2+} \Leftrightarrow \equiv S^{W2}ORa^+ + H^+$	log $K_1 = -5.0$

ionic strength as well as the pH edges at varying ionic strength indicate a similar but not always identical adsorption behavior of ^{226}Ra and Ba on montmorillonite. All experimental data could be quantitatively described by a cation exchange reaction with corresponding selectivity coefficients. In addition, to describe the uptake of Ba and Ra at high ionic strength and high pH, a surface complexation reaction on the amphoteric edge sites was considered with a best-fit surface complexation constant. The 2SPNE SC/CE model was applied for both elements, which reproduces the experimental data reasonably well. The adsorption was mainly dominated by a single cation exchange reaction of Ba^{2+} and Ra^{2+} with respect to Na^{+} on montmorillonite. The ion equilibria of Ba and ^{226}Ra on the planar sites could be modelled with one single cation exchange reaction, optimised for each dataset. To describe the more pronounced Ba and Ra uptake at high pH and IS, the surface complexation of Ba and Ra on edge sites was modelled by one single surface complexation constant, which was fixed in all model calculations.

The modelling results indicate that the contribution of this surface complex to the overall sorption is only becoming dominant at pH > 8 and combined with high ionic strength (NaCl concentration >0.1 M). At low ionic strength the selectivity coefficients for Ba and Ra are in good agreement (log K_c values vary between 0.70 and 0.84). At high ionic strength, the K_c (Ba–Na) was slightly higher compared to the low ionic strength data (log K_c of 0.90 (0.3 M) vs 0.70 (≤0.02 M)). In contrast, the K_c (Ra–Na) exhibits a clear dependency on ionic strength, with log K_c values of 0.7, 1.14 and 1.34 at NaCl concentrations of 0.01/0.02 M, 0.14 M and 0.3 M, respectively.

In conclusion, the results of this study indicate that Ba can be used as a good analogue for ^{226}Ra regarding the adsorption on montmorillonite at ionic strengths <0.1 M and pH < 8, but deviates in its behaviour at higher ionic strength. A plausible explanation for this observation could be the larger ionic radius of Ra compared to Ba which favours its selectivity behaviour on Na-montmorillonite. The contribution of surface complexation to the overall adsorption is the same for Ba and Ra and is independent of ionic strength. In addition to the newly obtained experimental ^{226}Ra adsorption data, the newly developed model was also tested against available literature data (Chen and Kocar, 2018) which are well predicted.

Declaration of competing interest

The authors declare that they have no known competing financial interests or personal relationships that could have appeared to influence the work reported in this paper.

Acknowledgements

This project has received funding from the European Union's Horizon 2020 research and innovation programme under grant agreement No 847593 (EURAD WP Future). We are grateful to K. Dahmen, M. Güngör and G. Modolo for their support.

Appendix

Table A 1
Experimental data of pH edges of ^{226}Ra (Fig. 1).

Experimental data					
I = 0.02 mol L^{-1}		I = 0.14 mol L^{-1}		I = 0.3 mol L^{-1}	
pH	log R_d	pH	log R_d	pH	log R_d
	(L kg^{-1})		(L kg^{-1})		(L kg^{-1})
5.51	3.99	5.58	2.19	5.65	1.69
5.52	3.98	5.59	2.15	5.60	1.70
6.28	3.61	6.30	2.23	6.09	1.67
6.25	3.62	6.30	2.21	6.14	1.67
6.97	3.77	6.95	2.25	6.83	1.70
6.95	3.80	6.97	2.24	6.85	1.76
8.48	3.01	8.59	2.55	8.25	1.98
8.44	3.02	8.16	2.47	8.38	2.05
9.17	3.39	9.20	2.70	9.09	2.38
9.14	3.28	9.21	2.70	9.10	2.39
9.81	3.40	9.88	2.97	9.01	2.30
9.79	3.41	10.2	3.00	9.20	2.41
9.88	2.97				
10.20	3.00				

Table A 2
Modelling pH edges of ^{226}Ra sorption at I = 0.01 mol L^{-1} (Chen and Kocar, 2018) (Fig. 1a).

Modelling ^{226}Ra sorption, I = 0.01 mol L^{-1}			
	model total	**planar sites (PS)**	**edge sites (ES)**
pH	log R_d (L kg^{-1})		
2.6	4.017	4.017	−7.387
2.8	4.095	4.095	−6.983
3.0	4.149	4.149	−6.581
3.2	4.184	4.184	−6.180
3.4	4.207	4.207	−5.779
3.6	4.222	4.222	−5.379
3.8	4.232	4.232	−4.980
4.0	4.238	4.238	−4.581
4.2	4.242	4.242	−4.183

(*continued on next page*)

Table A 2 (*continued*)

Modelling ^{226}Ra sorption, I = 0.01 mol L^{-1}			
4.4	4.245	4.245	−3.787
4.6	4.246	4.246	−3.393
4.8	4.247	4.247	−3.003
5.0	4.248	4.248	−2.618
5.2	4.248	4.248	−2.240
5.4	4.248	4.248	−1.873
5.6	4.249	4.249	−1.522
5.8	4.249	4.249	−1.189
6.0	4.249	4.249	−0.877
6.2	4.249	4.249	−0.589
6.4	4.249	4.249	−0.322
6.6	4.249	4.249	−0.074
6.8	4.249	4.249	0.160
7.0	4.249	4.249	0.382
7.2	4.249	4.249	0.597
7.4	4.249	4.249	0.807
7.6	4.249	4.249	1.013
7.8	4.249	4.249	1.216
8.0	4.249	4.249	1.418
8.2	4.250	4.249	1.619
8.4	4.250	4.249	1.819
8.6	4.251	4.249	2.017
8.8	4.253	4.249	2.215
9.0	4.255	4.249	2.410
9.2	4.259	4.249	2.602
9.4	4.264	4.249	2.790

Table A 3
Modelling pH edges of ^{226}Ra sorption at I = 0.02 mol L^{-1} (Fig. 1b).

Modelling ^{226}Ra sorption, I = 0.02 mol L^{-1}			
	model total	**planar sites (PS)**	**edge sites (ES)**
pH	log R_d (L kg^{-1})		
5.2	3.615	3.615	−2.302
5.4	3.615	3.615	−1.935
5.6	3.615	3.615	−1.583
5.8	3.615	3.615	−1.250
6.0	3.615	3.615	−0.939
6.2	3.615	3.615	−0.650
6.4	3.615	3.615	−0.383
6.6	3.615	3.615	−0.135
6.8	3.615	3.615	0.098
7.0	3.615	3.615	0.321
7.2	3.615	3.615	0.536
7.4	3.616	3.615	0.745
7.6	3.616	3.615	0.951
7.8	3.617	3.615	1.155
8.0	3.617	3.615	1.357
8.2	3.619	3.615	1.557
8.4	3.621	3.615	1.757
8.6	3.625	3.615	1.956
8.8	3.630	3.615	2.153
9.0	3.638	3.615	2.348
9.2	3.650	3.615	2.541
9.4	3.668	3.615	2.729
9.6	3.693	3.615	2.911
9.8	3.727	3.615	3.083
10.0	3.769	3.615	3.243
10.2	3.816	3.615	3.385
10.4	3.865	3.615	3.507

Table A 4
Modelling pH edges of ^{226}Ra sorption at I = 0.14 mol L^{-1} (Fig. 1c).

Modelling ^{226}Ra sorption, I = 0.14 mol L^{-1}			
	model total	**planar sites (PS)**	**edge sites (ES)**
pH	log R_d (L kg^{-1})		
5.2	2.240	2.240	−2.539
5.4	2.240	2.240	−2.172

(*continued on next page*)

Table A 4 (*continued*)

Modelling ^{226}Ra sorption, I = 0.14 mol L^{-1}			
5.6	2.240	2.240	−1.821
5.8	2.240	2.240	−1.488
6.0	2.240	2.240	−1.176
6.2	2.240	2.240	−0.888
6.4	2.241	2.240	−0.621
6.6	2.241	2.240	−0.372
6.8	2.242	2.240	−0.139
7.0	2.243	2.240	0.083
7.2	2.245	2.240	0.298
7.4	2.248	2.240	0.508
7.6	2.253	2.240	0.714
7.8	2.260	2.240	0.917
8.0	2.272	2.240	1.119
8.2	2.289	2.240	1.320
8.4	2.316	2.240	1.520
8.6	2.354	2.240	1.719
8.8	2.409	2.240	1.916
9.0	2.481	2.240	2.111
9.2	2.574	2.240	2.304
9.4	2.685	2.240	2.492
9.6	2.810	2.240	2.673
9.8	2.942	2.240	2.846
10.0	3.074	2.240	3.005
10.2	3.199	2.240	3.148
10.4	3.309	2.240	3.271

Table A 5
Modelling pH edges of ^{226}Ra sorption at I = 0.3 mol L^{-1} (Fig. 1d).

Modelling ^{226}Ra sorption, I = 0.3 mol L^{-1}			
	model total	**planar sites (PS)**	**edge sites (ES)**
pH	log R_d (L kg^{-1})		
5.2	1.731	1.731	−2.619
5.4	1.731	1.731	−2.253
5.6	1.731	1.731	−1.901
5.8	1.731	1.731	−1.568
6.0	1.732	1.731	−1.257
6.2	1.732	1.731	−0.968
6.4	1.733	1.731	−0.701
6.6	1.734	1.731	−0.453
6.8	1.736	1.731	−0.220
7.0	1.739	1.731	0.003
7.2	1.744	1.731	0.218
7.4	1.752	1.731	0.427
7.6	1.765	1.731	0.633
7.8	1.783	1.731	0.837
8.0	1.812	1.731	1.039
8.2	1.853	1.731	1.240
8.4	1.910	1.731	1.439
8.6	1.988	1.731	1.638
8.8	2.087	1.731	1.835
9.0	2.207	1.731	2.031
9.2	2.344	1.731	2.223
9.4	2.494	1.731	2.411

Table A 6
Experimental data of pH edges of ^{133}Ba (Fig. 2).

Ba sorption experimental data			
I = 0.03 mol L^{-1}		I = 0.3 mol L^{-1}	
pH	log R_d	pH	log R_d
	L kg^{-1}		L kg^{-1}
3.30	2.96	5.49	1.09
3.33	2.96	5.52	1.07
4.28	3.09	6.15	1.16
4.29	3.10	6.15	1.16
5.17	3.15	6.64	1.21
5.19	3.15	6.68	1.34

(*continued on next page*)

Table A 6 (*continued*)

Ba sorption experimental data			
$I = 0.03$ mol L^{-1}		$I = 0.3$ mol L^{-1}	
pH	log R_d	pH	log R_d
5.51	3.16	7.15	1.44
5.52	3.16	7.15	1.46
6.09	3.16	7.60	1.63
6.11	3.17	7.64	1.65
6.72	3.17	8.2	1.85
6.69	3.19	8.23	1.83
7.17	3.23	8.85	2.12
7.17	3.23	8.88	2.11
7.78	3.24	9.38	2.30
7.79	3.24	9.41	2.30
8.29	3.30	8.88	2.16
8.33	3.31	8.86	2.16
8.78	3.43	10.02	2.60
8.79	3.43	10.02	2.60
9.27	3.52	10.57	2.91
9.24	3.52	10.54	2.91

Table A 7
Modelling pH edges of ^{133}Ba sorption at $I = 0.03$ mol L^{-1} (Fig. 2a).

Modelling ^{133}Ba sorption, $I = 0.03$ mol L^{-1}			
	model total	**planar sites (PS)**	**edge sites (ES)**
pH	log R_d (L kg^{-1})		
3.2	3.224	3.224	−6.277
3.4	3.232	3.232	−5.877
3.6	3.237	3.237	−5.478
3.8	3.240	3.241	−5.078
4.0	3.243	3.243	−4.680
4.2	3.244	3.244	−4.282
4.4	3.245	3.245	−3.886
4.6	3.245	3.245	−3.492
4.8	3.246	3.246	−3.102
5.0	3.246	3.246	−2.717
5.2	3.246	3.246	−2.339
5.4	3.246	3.246	−1.973
5.6	3.246	3.246	−1.621
5.8	3.246	3.246	−1.288
6.0	3.246	3.246	−0.976
6.2	3.246	3.246	−0.688
6.4	3.246	3.246	−0.421
6.6	3.246	3.246	−0.173
6.8	3.246	3.246	0.061
7.0	3.247	3.246	0.283
7.2	3.247	3.246	0.498
7.4	3.247	3.246	0.708
7.6	3.248	3.246	0.914
7.8	3.249	3.246	1.117
8.0	3.251	3.246	1.319
8.2	3.254	3.246	1.520
8.4	3.259	3.246	1.720
8.6	3.266	3.246	1.918
8.8	3.277	3.246	2.115
9.0	3.294	3.246	2.311
9.2	3.318	3.246	2.503
9.4	3.353	3.246	2.691
9.6	3.400	3.246	2.873
9.8	3.458	3.246	3.046

Table A 8
Modelling of pH edges of ^{133}Ba sorption at $I = 0.3$ mol L^{-1} (Fig. 2b).

Modelling ^{133}Ba sorption, $I = 0.3$ mol L^{-1}			
	model total	**planar sites (PS)**	**edge sites (ES)**
pH	log R_d (L kg^{-1})		
5.0	1.321	1.321	−2.967
5.2	1.321	1.321	−2.590

(*continued on next page*)

Table A 8 (*continued*)

Modelling ^{133}Ba sorption, I = 0.3 mol L^{-1}			
5.4	1.321	1.321	−2.223
5.6	1.321	1.321	−1.871
5.8	1.322	1.321	−1.538
6.0	1.322	1.321	−1.227
6.2	1.323	1.321	−0.938
6.4	1.325	1.321	−0.671
6.6	1.329	1.321	−0.423
6.8	1.334	1.321	−0.190
7.0	1.343	1.321	0.033
7.2	1.356	1.321	0.247
7.4	1.377	1.321	0.457
7.6	1.407	1.321	0.663
7.8	1.452	1.321	0.867
8.0	1.514	1.321	1.069
8.2	1.597	1.321	1.269
8.4	1.702	1.321	1.469
8.6	1.829	1.321	1.668
8.8	1.974	1.321	1.865
9.0	2.133	1.321	2.060
9.2	2.301	1.321	2.253
9.4	2.473	1.321	2.441
9.6	2.644	1.321	2.623
9.8	2.809	1.321	2.795

Table A 9
Experimental data and model of isotherms of Ba and ^{226}Ra/^{133}Ba sorption at I = 0.02 mol L^{-1} (Fig. 3).

Experimental data						Model	
Ba			^{226}Ra/^{137}Ba				
log Ba_{eql}	log Ba_{ads}	log R_d	log$[Ba+Ra]_{eql}$	log R_d(Ra)	log R_d(Ba)	log Ba_{eql}	log R_d (Ra/Ba)
(mol L^{-1})	(mol/kg)	(L kg^{-1})	(mol L^{-1})	(L kg^{-1})	(L kg^{-1})	(mol L^{-1})	(L kg^{-1})
−1.81	−0.36	1.44	−1.84	1.87	1.53	−1.630	1.251
−1.81	−0.36	1.45	−1.84	1.87	1.53	−1.874	1.480
−2.03	−0.35	1.68	−2.07	1.97	1.62	−2.106	1.695
−2.03	−0.36	1.67	−2.08	1.97	1.68	−2.327	1.898
−2.33	−0.36	1.97	−2.39	2.23	2.25	−2.542	2.092
−2.33	−0.39	1.93	−2.39	2.22	2.27	−2.751	2.276
−2.49	−0.38	2.12	−2.54	2.32	2.19	−2.957	2.452
−2.50	−0.37	2.13	−2.55	2.33	2.19	−3.161	2.620
−2.91	−0.47	2.45	−2.93	2.57	2.52	−3.364	2.779
−2.92	−0.46	2.46	−2.94	2.57	2.54	−3.565	2.926
−3.42	−0.62	2.80	−3.46	2.95	2.78	−3.767	3.061
−3.42	−0.62	2.80	−3.47	2.93	2.77	−3.967	3.181
−3.89	−0.83	3.07	−3.93	3.22	3.01	−4.168	3.285
−3.90	−0.82	3.08	−3.93	3.22	3.01	−4.368	3.372
−4.29	−1.06	3.23	−4.34	3.44	3.36	−4.569	3.441
−4.30	−1.06	3.24	−4.35	3.44	3.38	−4.769	3.495
−4.66	−1.33	3.33	−4.54	3.20	3.17	−4.969	3.534
−5.13		3.39	−4.55	3.20	3.19	−5.169	3.561
−5.07	−1.74	3.31	−5.00	3.32	3.22	−5.369	3.580
−5.67	−1.76	3.42	−5.02	3.31	3.25	−5.569	3.593
−5.63	−2.25	3.38	−5.65	3.32	3.48	−5.769	3.601
−6.63	−2.26	3.47	−5.58	3.32	3.40	−5.969	3.606
−7.18	−3.16	3.51	−6.66	3.30	3.56	−6.169	3.609
−7.17		3.49	−6.65	3.30	3.54	−6.369	3.612
−7.85	−3.68	3.53	−7.38	3.61	3.75	−6.569	3.613
−7.85	−3.68	3.52	−7.75	3.65	4.19	−6.769	3.614
−8.28	−4.34	3.53	−7.67	3.59	3.28	−6.969	3.614
−8.30	−4.34	3.55	−7.67	3.61	3.28	−7.169	3.615
−8.66	−4.79	3.54	−7.85	3.61		−7.369	3.615
−8.66	−4.79	3.54	−7.90	3.62		−7.569	3.615
	−5.20		−8.90	3.59		−7.769	3.615
	−5.20		−8.91	3.61		−7.969	3.615
						−8.169	3.615
						−8.369	3.615
						−8.569	3.615
						−8.769	3.615
						−8.969	3.615
						−9.169	3.615

Appendix A. Supplementary data

Supplementary data to this article can be found online at https://doi.org/10.1016/j.apgeochem.2021.105117.

References

Ames, L.L., McGarrah, J.E., Walker, B.A., 1983. Sorption of trace constituents from aqueous solutions onto secondary minerals. II. Radium. Clays Clay Miner. 31, 335–342. https://doi.org/10.1346/CCMN.1983.0310502.

Baeyens, B., Bradbury, M.H., 1995. Technical Report 95-05: A Quantitative Mechanistic Description of Ni, Zn and Ca Sorption on Na-Montmorillonite Part 11: Sorption Measurements. Villigen PSI, Switzerland.

Baeyens, B., Bradbury, M.H., 1997. A mechanistic description of Ni and Zn sorption on Na-montmorillonite Part I: titration and sorption measurements. J. Contam. Hydrol. 27, 199–222. https://doi.org/10.1016/S0169-7722(97)00008-9.

Boscov, M., Cunha, I., Saita, R., 2001. Radium migration through clay liners at waste disposal sites. Sci. Total Environ. 266, 259–264. https://doi.org/10.1016/S0048-9697(00)00755-5.

Bradbury, M.H., Baeyens, B., 1997. A mechanistic description of Ni and Zn sorption on Na-montmorillonite Part II: modelling. J. Contam. Hydrol. 27, 223–248. https://doi.org/10.1016/S0169-7722(97)00007-7.

Bradbury, M.H., Baeyens, B., 2005. Modelling the sorption of Mn(II), Co(II), Ni(II), Zn (II), Cd(II), Eu(III), Am(III), Sn(IV), Th(IV), Np(V) and U(VI) on montmorillonite: linear free energy relationships and estimates of surface binding constants for some selected heavy metals and actinide. Geochem. Cosmochim. Acta 69, 875–892. https://doi.org/10.1016/j.gca.2004.07.020.

Chen, M.A., Kocar, B.D., 2018. Radium sorption to iron (Hydr)oxides, pyrite, and montmorillonite: implications for mobility. Environ. Sci. Technol. 52, 4023–4030. https://doi.org/10.1021/acs.est.7b05443.

Curti, E., Fujiwara, K., Iijima, K., Tits, J., Cuesta, C., Kitamura, A., Glaus, M.a., Müller, W., 2010. Radium uptake during barite recrystallization at 23±2°C as a function of solution composition: an experimental 133Ba and 226Ra tracer study. Geochem. Cosmochim. Acta 74, 3553–3570. https://doi.org/10.1016/j.gca.2010.03.018.

Davies, C.W., 1962. Ion Association. Butterworths.

Ewing, R.C., 2015. Long-term storage of spent nuclear fuel. Nat. Mater. 14, 252–257. https://doi.org/10.1038/nmat4226.

Fernandes, M.M., Baeyens, B., 2019. Cation exchange and surface complexation of lead on montmorillonite and illite including competitive adsorption effects. Appl. Geochem. 100, 190–202. https://doi.org/10.1016/j.apgeochem.2018.11.005.

Fisher, R.S., 1998. Geologic and geochemical controls on naturally occurring radioactive materials (NORM) in produced water from oil, gas, and geothermal operations. Environ. Geosci. 5, 139–150.

Gaines, G.L., Thomas, H.C., 1955. Adsorption studies on clay minerals. V. Montmorillonite-cesium-strontium at several temperatures. J. Chem. Phys. 23, 2322–2326. https://doi.org/10.1063/1.1741873.

Gusa, A.V., Tomani, A., Zhang, Z., Vidic, R.D., 2020. Sulfate precipitation in produced water from Marcellus Shale for the control of naturally occurring radioactive material. Water Res. 177, 115765. https://doi.org/10.1016/j.watres.2020.115765.

Heberling, F., Metz, V., Böttle, M., Curti, E., Geckeis, H., 2018. Barite recrystallization in the presence of 226Ra and 133Ba. Geochem. Cosmochim. Acta 232, 124–139. https://doi.org/10.1016/j.gca.2018.04.007.

Hidaka, H., Horie, K., Gauthier-Lafaye, F., 2007. Transport and selective uptake of radium into natural clay minerals. Earth Planet Sci. Lett. 264, 167–176. https://doi.org/10.1016/j.epsl.2007.09.027.

Jenni, A., Wersin, P., Thoenen, T., Baeyens, B., Ferrari, A., Gimmi, T., Mäder, U., Marschall, P., Hummel, W., Leupin, O., 2019. Bentonite Backfill Performance in a High-Level Waste Repository: a Geochemical Perspective (Nagra: Technical Report, Report No.: NTB 19-03).

Klinkenberg, M., Weber, J., Barthel, J., Vinograd, V., Poonoosamy, J., Kruth, M., Bosbach, D., Brandt, F., 2018. The solid solution–aqueous solution system (Sr,Ba,Ra) SO_4 + H_2O: a combined experimental and theoretical study of phase equilibria at Sr-rich compositions. Chem. Geol. 497, 1–17. https://doi.org/10.1016/j.chemgeo.2018.08.009.

Komarneni, S., Kozai, N., Paulus, W.J., 2001. Superselective clay for radium uptake. Nature 410, 771. https://doi.org/10.1038/35071173, 771.

Marcus, Y., 1991. Thermodynamics of solvation of ions. Part 5. - Gibbs free energy of hydration at 298.15 K. J. Chem. Soc., Faraday Trans. 87, 2995–2999. https://doi.org/10.1039/FT9918702995.

Martin, A.J., Crusius, J., McNee, J.J., Yanful, E.K., 2003. The mobility of radium-226 and trace metals in pre-oxidized subaqueous uranium mill tailings. Appl. Geochem. 18, 1095–1110. https://doi.org/10.1016/S0883-2927(02)00243-3.

Nagra, 2002. Project Opalinus Clay: Safety Report. Demonstration of Disposal Feasibility (Entsorgungsnachweis) for Spent Fuel, Vitrified High-Level Waste and Long-Lived Intermediate-Level Waste. Technical Report NTB 02-05. Wettingen, Switzerland.

Nagra, 2014. Modellhaftes Inventar für radioaktive Materialien MIRAM 14. Wettingen, Switzerland.

Rosenberg, Y.O., Sadeh, Y., Metz, V., Pina, C.M., Ganor, J., 2014. Nucleation and growth kinetics of RaxBa1-xSO4 solid solution in NaCl aqueous solutions. Geochem. Cosmochim. Acta 125, 290–307. https://doi.org/10.1016/j.gca.2013.09.041.

Rutherford, P., Dudas, M., Arocena, J., 1996. Heterogeneous distribution of radionuclides, barium and strontium in phosphogypsum by-product. Sci. Total Environ. 180, 201–209.

Silva, C., Heilbron Filho, P.F.L., Pérez Guerrero, J.S., Xavier, A.M., Pereira, G.C., Lacerda, G.B.M., Pimentel, L.C.G., Landau, L., Ebecken, N.F.F., 2020. A computational model for estimation of 226Ra and 228Ra concentrations in sludge from petrol exploitation, based on radiation-level measurements on stored packages. Environ. Earth Sci. 79, 489. https://doi.org/10.1007/s12665-020-09237-3.

Shannon, R.D., 1976. Revised effective ionic radii and systematic studies of interatomic distances in halides and chalcogenides. Acta Crystallogr. A 32 (5), 751–767. https://doi.org/10.1107/S0567739476001551.

SKB, 2011. Long-term Safety for the Final Repository of Spent Nuclear Fuel at Forsmark Main Report of the Sr-Site Project I-III. Stockholm, Sweden.

Society, T.C.M.. https://www.clays.org/sourceclays_data/.

Tachi, Y., Shibutani, T., Sato, H., Yui, M., 2001. Experimental and modeling studies on sorption and diffusion of radium in bentonite. J. Contam. Hydrol. 47, 171–186. https://doi.org/10.1016/S0169-7722(00)00147-9.

Teppen, B.J., Miller, D.M., 2006. Hydration Energy Determines Isovalent Cation Exchange Selectivity by Clay Minerals. Soil Science Society of America Journal. https://doi.org/10.2136/sssaj2004.0212.

Tertre, E., Ferrage, E., Bihannic, I., Michot, L.J., Prêt, D., 2011a. Influence of the ionic strength and solid/solution ratio on Ca(II)-for-Na+ exchange on montmorillonite. Part 2: understanding the effect of the m/V ratio. Implications for pore water composition and element transport in natural media. J. Colloid Interface Sci. 363 (1), 334–347. https://doi.org/10.1016/j.jcis.2011.07.003.

Tertre, E., Prêt, D., Ferrage, E., 2011b. Influence of the ionic strength and solid/solution ratio on Ca(II)-for-Na+ exchange on montmorillonite. Part 1: chemical measurements, thermodynamic modeling and potential implications for trace elements geochemistry. J. Colloid Interface Sci. 353 (1), 248–256. https://doi.org/10.1016/j.jcis.2010.09.039.

Van Loon, L.R., Glaus, M.A., 2008. Mechanical Compaction of Smectite Clays Increases Ion Exchange Selectivity for Cesium. Environmental Science and Technology. https://doi.org/10.1021/es702487m.

Van Olphen, H., Fripiat, J.J., 1979. Data Handbook for Clay Materials and Other Non-metallic Minerals, first ed. Pergamon Press, Oxford, New York, Toronto, Sydney, Paris, Frankfurt, p. 346.

Westall, J.C., Zachary, J.L., Morel, F.M.M., 1976. Mineql - general algorithm for computation of chemical-equilibirum in aqueous systems. In: Abstracts of Papers of the American Chemical Society. American Chemical Society, Washington, D.C., p. 8, 8.

Zhang, T., Hammack, R.W., Vidic, R.D., 2015. Fate of radium in marcellus shale flowback water impoundments and assessment of associated health risks. Environ. Sci. Technol. 49, 9347–9354. https://doi.org/10.1021/acs.est.5b01393.